BRAIN COMMUNICATIONS

CYP46A1-dependent and independent effects of efavirenz treatment

Natalia Mast, Nicole El-Darzi, Alexey M. Petrov,* Young Li and Irina A. Pikuleva

Cholesterol excess in the brain is mainly disposed *via* cholesterol 24-hydroxylation catalysed by cytochrome P450 46A1, a CNS-specific enzyme. Cytochrome P450 46A1 is emerging as a promising therapeutic target for various brain diseases with both enzyme activation and inhibition having therapeutic potential. The rate of cholesterol 24-hydroxylation determines the rate of brain cholesterol turnover and the rate of sterol flux through the plasma membranes. The latter was shown to affect membrane properties and thereby membrane proteins and membrane-dependent processes. Previously we found that treatment of 5XFAD mice, an Alzheimer's disease model, with a small dose of anti-HIV drug efavirenz allosterically activated cytochrome P450 46A1 in the brain and mitigated several disease manifestations. Herein, we generated *Cyp46a1*$^{-/-}$5XFAD mice and treated them, along with 5XFAD animals, with efavirenz to ascertain cytochrome P450 46A1-dependent and independent drug effects. Efavirenz-treated versus control *Cyp46a1*$^{-/-}$5XFAD and 5XFAD mice were compared for the brain sterol and steroid hormone content, amyloid β burden, protein and mRNA expression as well as synaptic ultrastructure. We found that the cytochrome P450 46A1-dependent efavirenz effects included changes in the levels of brain sterols, steroid hormones, and such proteins as glial fibrillary acidic protein, Iba1, Munc13-1, post-synaptic density-95, gephyrin, synaptophysin and synapsin-1. Changes in the expression of genes involved in neuroprotection, neurogenesis, synaptic function, inflammation, oxidative stress and apoptosis were also cytochrome P450 46A1-dependent. The total amyloid β load was the same in all groups of animals, except lack of cytochrome P450 46A1 decreased the production of the amyloid β40 species independent of treatment. In contrast, altered transcription of genes from cholinergic, monoaminergic, and peptidergic neurotransmission, steroid sulfation and production as well as vitamin D_3 activation was the main CYP46A1-independent efavirenz effect. Collectively, the data obtained reveal that CYP46A1 controls cholesterol availability for the production of steroid hormones in the brain and the levels of biologically active neurosteroids. In addition, cytochrome P450 46A1 activity also seems to affect the levels of post-synaptic density-95, the main postsynaptic density protein, possibly by altering the calcium/calmodulin-dependent protein kinase II inhibitor 1 expression and activity of glycogen synthase kinase 3β. Even at a small dose, efavirenz likely acts as a transcriptional regulator, yet this regulation may not necessarily lead to functional effects. This study further confirmed that cytochrome P450 46A1 is a key enzyme for cholesterol homeostasis in the brain and that the therapeutic efavirenz effects on 5XFAD mice are likely realized *via* cytochrome P450 46A1 activation.

Department of Ophthalmology and Visual Sciences, Case Western Reserve University, Cleveland, OH, USA

*Present address: Laboratory of Biophysics of Synaptic Processes, Kazan Institute of Biochemistry and Biophysics, Federal Research Center "Kazan Scientific Center of RAS", 2/31 Lobachevsky Street, box 30, 420111, Kazan, Russia; and Institute of Neuroscience, Kazan State Medial University, 49 Butlerova Street, 420012, Kazan, Russia

Correspondence to: Irina A. Pikuleva, Department of Ophthalmology and Visual Sciences, Case Western Reserve University, 2085 Adelbert Rd., Room 303, Cleveland, OH 44106, USA
E-mail address: iap8@case.edu

Keywords: Alzheimer's disease; brain; cholesterol; CYP46A1; membrane properties

Received July 28, 2020. Revised September 22, 2020. Accepted October 5, 2020. Advance Access publication October 29, 2020

Graphical Abstract

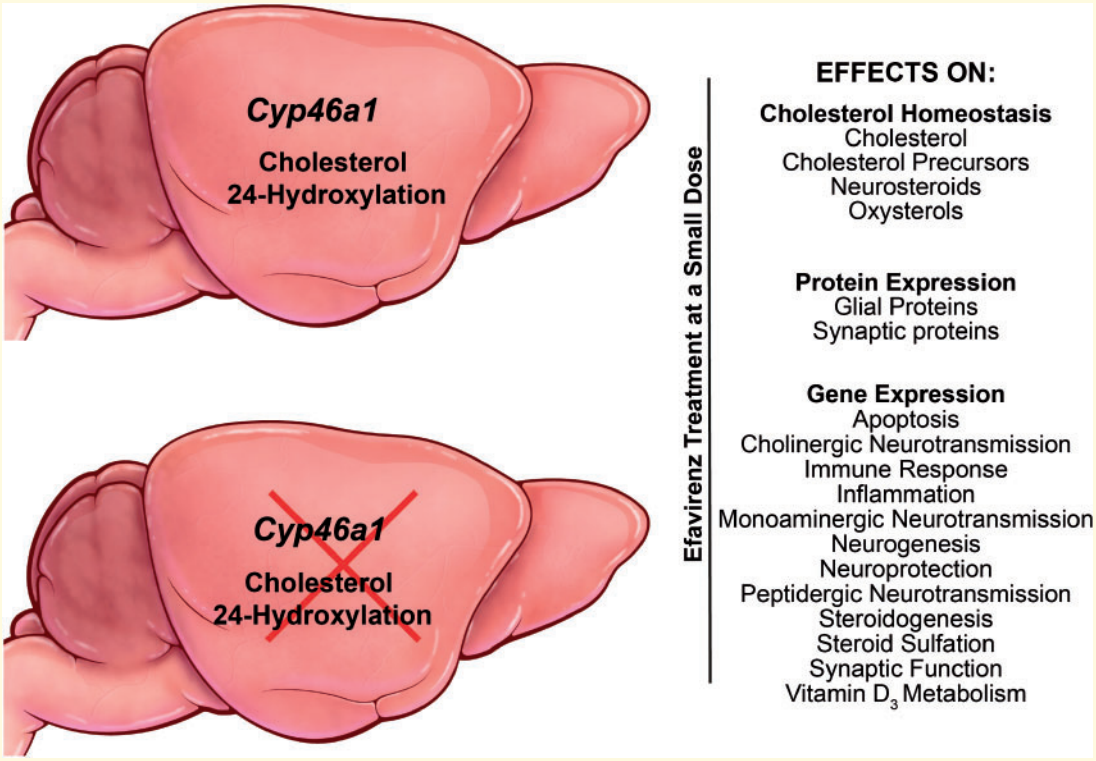

Abbreviations: Aβ = amyloid β peptide; C25H = cholesterol 25-hydroxylase; CYP46A1 = cytochrome P450 46A1; DHEA = dehydroepiandrosterone; EFV = efavirenz; PSD-95 = post-synaptic density-95; RNA-Seq = whole transcriptome sequencing; ThioS = Thioflavin S

Introduction

The main pathway of cholesterol elimination in the brain is initiated by cytochrome P450 46A1 (CYP46A1), which is normally expressed in neurons (Ramirez *et al.*, 2008) and ectopically in astrocytes or microglia (Brown *et al.*, 2004; Cartagena *et al.*, 2008; Petrov *et al.*, 2019a). CYP46A1 converts cholesterol to 24-hydroxycholesterol (24HC), a transportable form of cholesterol from the brain into the systemic circulation and a biologically active oxysterol that can interact with different proteins and receptors such as liver X receptors and *N*-methyl-D-aspartate receptors (Lutjohann *et al.*, 1996; Bjorkhem *et al.*, 1998; Janowski *et al.*, 1999; Lund *et al.*, 1999; Meaney *et al.*, 2002; Paul *et al.*, 2013). Studies in mice showed that increases in CYP46A1 activity by genetic or pharmacologic means are beneficial in the models of Alzheimer's and Huntington's diseases, Niemann–Pick disease type C, spinocerebellar ataxia, depression and glioblastoma (Hudry *et al.*, 2010; Burlot *et al.*, 2015; Boussicault *et al.*, 2016; Mast *et al.*, 2017b; Patel *et al.*, 2017; Han *et al.*, 2019; Kacher *et al.*, 2019; Mitroi *et al.*, 2019; Nóbrega *et al.*, 2019; Petrov *et al.*, 2019b). A clinical trial is on-going in people with Alzheimer's disease to evaluate CYP46A1 activation by efavirenz (EFV), a reverse transcriptase inhibitor and anti-HIV drug (ClinicalTrials.gov, NCT03706885). Another clinical trial is also in progress (ClinicalTrials.gov, NCT03650452) to test whether CYP46A1 inhibition by soticlestat (TAK-935/OV935), an experimental pharmaceutical, will mitigate excessive neuronal excitation in children with frequent seizures due to rare genetic diseases.

Modulation of CYP46A1 activity in animal studies was found to affect various biological processes (Hudry *et al.*, 2010; Burlot *et al.*, 2015; Boussicault *et al.*, 2016; Kacher *et al.*, 2019; Mitroi *et al.*, 2019; Nóbrega *et al.*, 2019). Hence, we proposed the sterol flux hypothesis as sterol flux was a common process modulated in the brain of these animals (Petrov *et al.*, 2020). Indeed, enhanced CYP46A1 activity or CYP46A1 lack lead to a compensatory increase and decrease, respectively, in the rates of cholesterol biosynthesis and turnover and thereby the rate of sterol flux through the plasma membranes (Lund *et al.*, 2003; Mast *et al.*, 2017b; Petrov *et al.*, 2019a).

The latter in turn could alter the physico-chemical properties of the plasma membranes and membrane-dependent events (Petrov *et al.*, 2020), thus unifying the multiple CYP46A1 activity effects. Studies on synaptosomal fractions isolated from the brain of mice with increased and decreased sterol fluxes provided support for this hypothesis by showing opposite changes in membrane ordering, thickness, resistance to osmotic stress and cholesterol accessibility. Also, the rate of sterol flux was found to affect the exocytotic glutamate release and protein phosphorylation *via* changes in the activity of different protein kinases and phosphatases (Petrov *et al.*, 2020).

The on-going clinical trial of EFV in patients with Alzheimer's disease is based on our preclinical studies of 5XFAD mice (an Alzheimer's disease model), which received the drug at 0.1 mg/kg of body weight/day, a much smaller dose than that given to HIV-positive individuals (600 mg/day). The drug administration was either from 1 to 9 months of age, denoted as the first treatment paradigm, or from 3 to 9 months of age, denoted as the second treatment paradigm (Mast *et al.*, 2017b; Petrov *et al.*, 2019a). In both treatments, EFV enhanced CYP46A1 activity, increased brain cholesterol turnover, and improved mouse performance in the Morris water maze test. The effects on the amyloid β levels (Aβ), astrocyte and microglia activation and expression of essential synaptic proteins were the treatment paradigm-specific (Petrov *et al.*, 2019b) with both age (or initial Aβ load) and treatment duration appearing to determine in part the outcome of treatment.

When given to humans daily at 600 mg, EFV carries a risk of neuropsychiatric complications, usually mild to moderate and often transient, and alters the plasma lipid profile (Sension and Deckx, 2015; Dalwadi *et al.*, 2016). Some of these effects could be reproduced in rodents at drug doses $\geq$10 mg/kg body weight/day (Tohyama *et al.*, 2009; Apostolova *et al.*, 2015, 2017). The mechanisms for EFV side effects are not totally clear but are suggested to include its interactions with specific neurotransmitter and nuclear receptors (Faucette *et al.*, 2007; Gatch *et al.*, 2013; Sharma *et al.*, 2013; Dalwadi *et al.*, 2016; Narayanan *et al.*, 2018). Accordingly, even at a very small dose, as that used in our studies, EFV can still interact with proteins other than CYP46A1 and elicit CYP46A1-independent effects. Therefore, herein, we generated *Cyp46a1*$^{-/-}$5XFAD mice which lacked CYP46A1 and hypothesized that CYP46A1-dependent effects should only be observed in EFV-treated 5XFAD mice, whereas CYP46A1-independent effects will be present in both EFV-treated 5XFAD and *Cyp46a1*$^{-/-}$5XFAD animals. Also, we assumed that the Aβ load will not confound our *Cyp46a1*$^{-/-}$5XFAD to 5XFAD mice comparisons as *Cyp46a1* ablation did not affect amyloid formation in another mouse model of Alzheimer's disease (Halford and Russell, 2009). Indeed, we identified CYP46A1-dependent and independent effects of EFV treatment and unexpectedly revealed new CYP46A1 roles in the brain.

Materials and methods

Animals

5XFAD$^{Tg/0}$ mice are hemizygous for the mutant (K670N, M671L, I716V and V717I) human amyloid precursor protein 695 and mutant (M146L and L286V) human presenilin 1. This genotype was obtained by crossing 5XFAD$^{Tg/0}$ males with wild type B6SJL females, both of which were from The Jackson Laboratory. Only F1 generation of hemizygous animals was then used, which start to develop Aβ deposits and behavioural deficits from 2 and 4 months of age, respectively (Oakley *et al.*, 2006; Ohno *et al.*, 2006). *Cyp46a1*$^{-/-}$ females were obtained as described (Mast *et al.*, 2017a) from *Cyp46a1*$^{+/-}$ mice on the mixed C57BL/6J; 129S6/SvEv background provided by Dr. David Russell (UT Southwestern) (Lund *et al.*, 2003). *Cyp46a1*$^{-/-}$ females were crossed with F1 5XFAD$^{Tg/0}$ males and then *Cyp46a*$^{+/-}$5XFAD$^{Tg/0}$ mice were crossed to one another to obtain *Cyp46a1*$^{-/-}$5XFAD$^{Tg/0}$ mice. EFV treatment was as described for the second treatment paradigm (Petrov *et al.*, 2019a), i.e., from 3 to 9 months of age at a 0.1 mg/kg body weight/day drug dose delivered in drinking water. All animals were maintained in a temperature and humidity-controlled environment with 12-h light–dark cycle with standard rodent chow and water provided *ad libitum*. All animal experiments were approved by the Institutional Animal Care and Use Committee and conformed to recommendations of the American Veterinary Association Panel on Euthanasia. Both female and male mice were used. Littermates were selected from the pool of all available animals and randomly assigned to either the control or treatment group, which were matched by size, age (3 months old) and gender. Sample size was based on previous experience. Experimenters were not blinded with respect to mouse genotype or EFV treatment.

Brain processing

This was as described (Petrov *et al.*, 2019a) after an overnight fasting. Briefly, if used for histochemistry, i.e. Thioflavin S (ThioS) stains, mice were anaesthetized and perfused through the heart with phosphate buffer saline (30 ml, 1 ml/min) followed by 4% paraformaldehyde in phosphate buffer saline (30 ml, 1 ml/min). For all other experiments, mice were euthanized by cervical dislocation. The brains were rinsed in cold phosphate buffer saline, blotted, and dissected along the midline following removal of both the cerebellum and brainstem. Right hemispheres were designated for sterol quantifications, western blots or whole transcriptome sequencing (RNA-Seq), whereas left hemispheres were always used for Aβ peptide measurements by ELISA, qRT-PCR or ultrastructural analysis of synaptosomal fractions by transmission electron microscopy. These hemisphere assignments were random but consistent within the study. The isolation of

synaptosomal fractions, ThioS stains, western blots, ELISA (Human Aβ40 and Aβ42 ELISA kits, Invitrogen, KHB3481 and KHB3441, respectively), qRT-PCR and transmission electron microscopy were all carried out as described (Mast *et al.*, 2017b; Petrov *et al.*, 2019a; Petrov *et al.*, 2020). The antibodies and primers used are summarized in Supplementary Tables 1and 2.

Sterol quantifications

Free and total content (the latter is a sum of the unesterified and either esterified or sulfated form) were measured by gas chromatography-mass spectroscopy using deuterated sterol analogues as internal standards (Mast *et al.*, 2011). A cohort of control and EFV-treated 5XFAD mice different from that described previously (Petrov *et al.*, 2019a) was used for these measurements. Sample saponification to determine the esterified sterol content or solvolysis to measure the extent of the sterol sulfation were as described (Liere *et al.*, 2004; Mast *et al.*, 2011).

Histochemistry

ThioS stains were with 1% aqueous solution (Sigma-Aldrich) as described (Mast *et al.*, 2017b). All images were acquired on a NanoZoomer S60 Digital slide scanner (Hamamatsu) and were analysed by the QuPath (v0.2.0 M9) software (Bankhead *et al.*, 2017) for the total number and combined area of the ThioS-positive cells. Only signals at a threshold of 25 arbitrary units, a shape factor of $\geq$0.2, and the size of plaques from 50 to 200 μm^2 were considered for the quantifications.

RNA-Seq

This was conducted on brain homogenates by BGI Americas as described (Jiang *et al.*, 2020; Zhou *et al.*, 2020). See Supplementary material for details.

Statistical analysis

Data from all available brains were used. There were no exclusion of statistical outliers. Data represent the mean $\pm$ SD; the sample size is indicated in each figure or figure legend. Either a two-tailed, unpaired Student's *t*-test, two-way ANOVA followed by Bonferroni *post hoc* comparisons or mixed-effects model from the GraphPad Prism (GraphPad) software were used. Statistical significance was defined as $^{*}P \leq 0.05$; $^{**}P \leq 0.01$; $^{***}P \leq 0.001$.

Data availability

The authors confirm that the data supporting the findings of this study are available upon request.

Results

Brain sterol levels

Cholesterol, 24-hydroxycholesterol and 13 other sterols, which are present in the brain (Fig. 1), were quantified in five groups of animals: B6SJL mice, a background strain for 5XFAD mice; control 5XFAD mice; EFV-treated 5XFAD mice; control *Cyp46a1*$^{-/-}$5XFAD mice; and EFV-treated *Cyp46a1*$^{-/-}$5XFAD mice (Fig. 2A). We also measured cholesterol and steroid sulfation, cholesterol esterification as well as sitosterol and campesterol, the dietary plant sterols and markers of the integrity of the blood–brain barrier, which is normally impermeable to cholesterol (Lütjohann *et al.*, 2002; Vanmierlo *et al.*, 2012).

The sitosterol and campesterol levels were low in the brain of B6SJL mice but increased more than 3- and 70-fold in the brain of control 5XFAD and *Cyp46a1*$^{-/-}$5XFAD mice, respectively. EFV treatment reduced the sitosterol levels in 5XFAD mice (by 24%) but not in *Cyp46a1*$^{-/-}$5XFAD mice and had no effect on campesterol levels. Apparently, both lines of control and EFV-treated transgenic animals had a dysfunction of the blood–brain barrier.

Lathosterol and desmosterol are the cholesterol precursors (Fig. 1) and markers of cholesterol biosynthesis in the neurons and astrocytes, respectively (Nieweg *et al.*, 2009). In control 5XFAD versus B6SJL mice, the levels of lathosterol and desmosterol were increased, whereas in control *Cyp46a1*$^{-/-}$5XFAD mice versus B6SJL mice, the lathosterol and desmosterol content was decreased (Fig. 2A). EFV treatment further increased the lathosterol and desmosterol levels in 5XFAD mice and had no effect on the lathosterol levels in *Cyp46a1*$^{-/-}$5XFAD mice, while decreasing their desmosterol levels. Thus, mechanistically, control 5XFAD mice had an upregulation of the brain cholesterol biosynthesis, whereas control *Cyp46a1*$^{-/-}$5XFAD mice had a cholesterol biosynthesis decrease (Fig. 2B). EFV treatment enhanced CYP46A1-mediated cholesterol elimination and thereby further increased cholesterol biosynthesis in 5XFAD mice (Fig. 2C) but had an opposite effect on cholesterol biosynthesis in *Cyp46a1*$^{-/-}$5XFAD mice (Fig. 2D).

In the brain, cholesterol is mainly present in the free form with esterified and sulfated forms representing less than 10% and 0.1% of the total cholesterol content, respectively (Liu *et al.*, 2003; Björkhem and Meaney, 2004; Karu *et al.*, 2007). B6SJL, control 5XFAD and control *Cyp46a1*$^{-/-}$5XFAD mice had similar content of free, esterified and sulfated cholesterol, and free cholesterol was the major sterol form in these groups (Fig. 2A). EFV treatment did not affect the levels of free and esterified cholesterol in 5XFAD mice, but significantly decreased the levels of free and hence total cholesterol in *Cyp46a1*$^{-/-}$5XFAD mice. Apparently, EFV treatment did not disturb cholesterol homeostasis in 5XFAD mice as

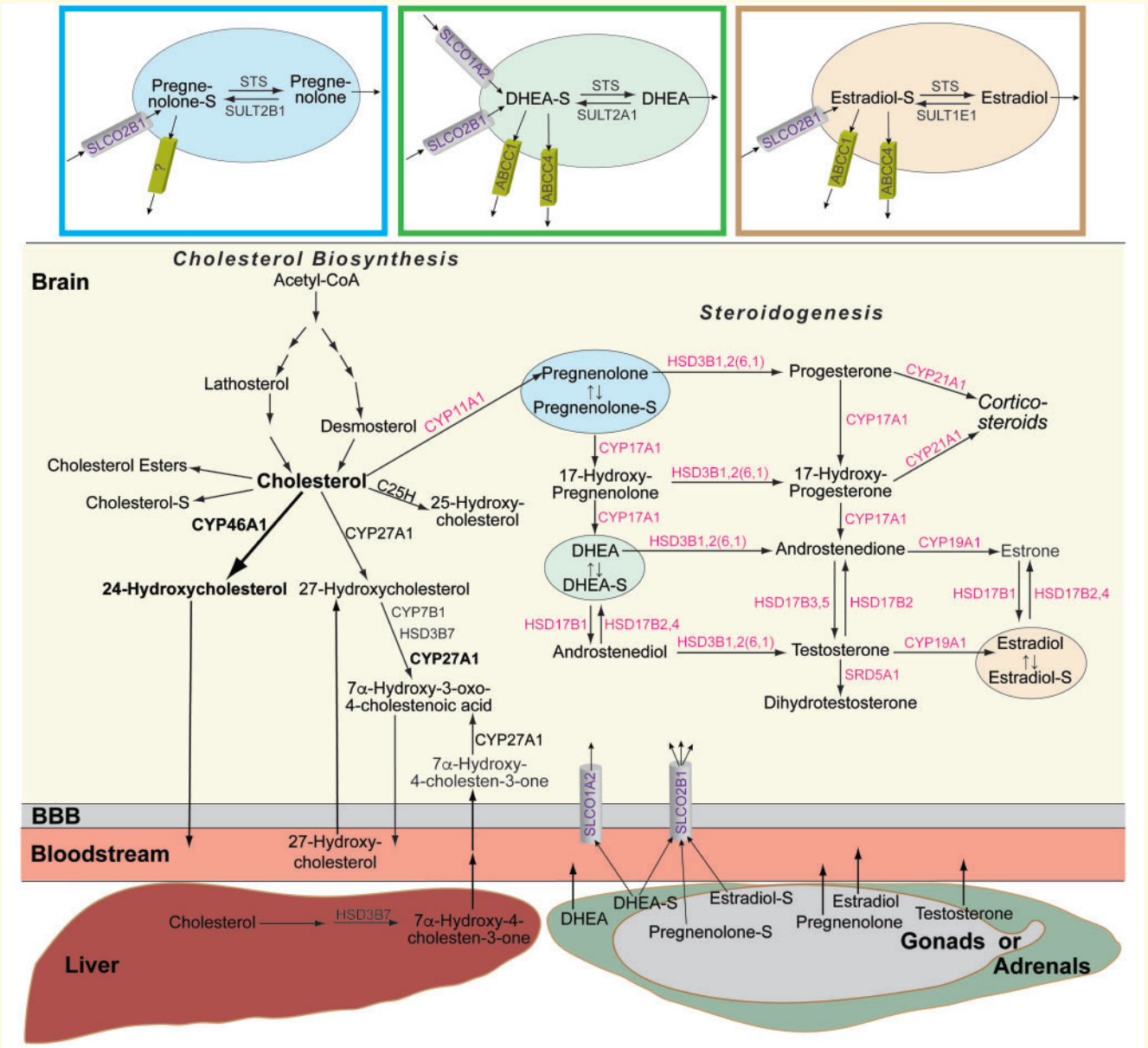

Figure 1 Brain pathways of cholesterol input, output and steroidogenesis evaluated in the present work. Bold arrow and font indicate the quantitatively major pathway of cholesterol metabolism in the brain. Enzymes in black over arrows are those involved in cholesterol input and output in the brain (Mast *et al.*, 2017a); enzymes in magenta are those involved in neurosteroidogenesis (Mellon and Griffin, 2002). Numbers in parenthesis indicate orthologous isoforms in mice, if the mouse isoform is different from that of a human orthologue. Coloured boxes show the major proteins that determine the cellular levels of sulfated steroids (Mueller *et al.*, 2015). BBB = blood-brain barrier. Cholesterol-S, pregnenolone-S, DHEA-S and estradiol-S are cholesterol sulfate, pregnenolone sulfate, dehydroepiandrosterone sulfate and oestradiol sulfate, respectively.

they continued to maintain the same steady-state cholesterol levels as control 5XFAD mice but dysregulated cholesterol homeostasis in *Cyp46a1*$^{-/-}$5XFAD mice (Fig. 2C, D).

24-Hydroxycholesterol, the CYP46A1 product, was present at the same levels in B6SJL and control 5XFAD mice but was not detectable in control *Cyp46a1*$^{-/-}$5XFAD mice, which do not express CYP46A1 (Fig. 2A). EFV treatment increased the 24-hydroxycholesterol levels in 5XFAD mice and did not lead to any detectable 24-hydroxycholesterol in *Cyp46a1*$^{-/-}$5XFAD mice. Thus, we confirmed our previous findings (Mast *et al.*, 2017b; Petrov *et al.*, 2019a) that EFV treatment activates CYP46A1 in 5XFAD mice and that in our *Cyp46a1*$^{-/-}$5XFAD mice, functional CYP46A1 was indeed absent.

CYP27A1 catalyses the C27-hydroxylation of different sterols including cholesterol (Wikvall, 1984; Okuda *et al.*, 1988) (Fig. 1). Normally, 27-hydroxycholesterol does not flux from the brain into the systemic circulation

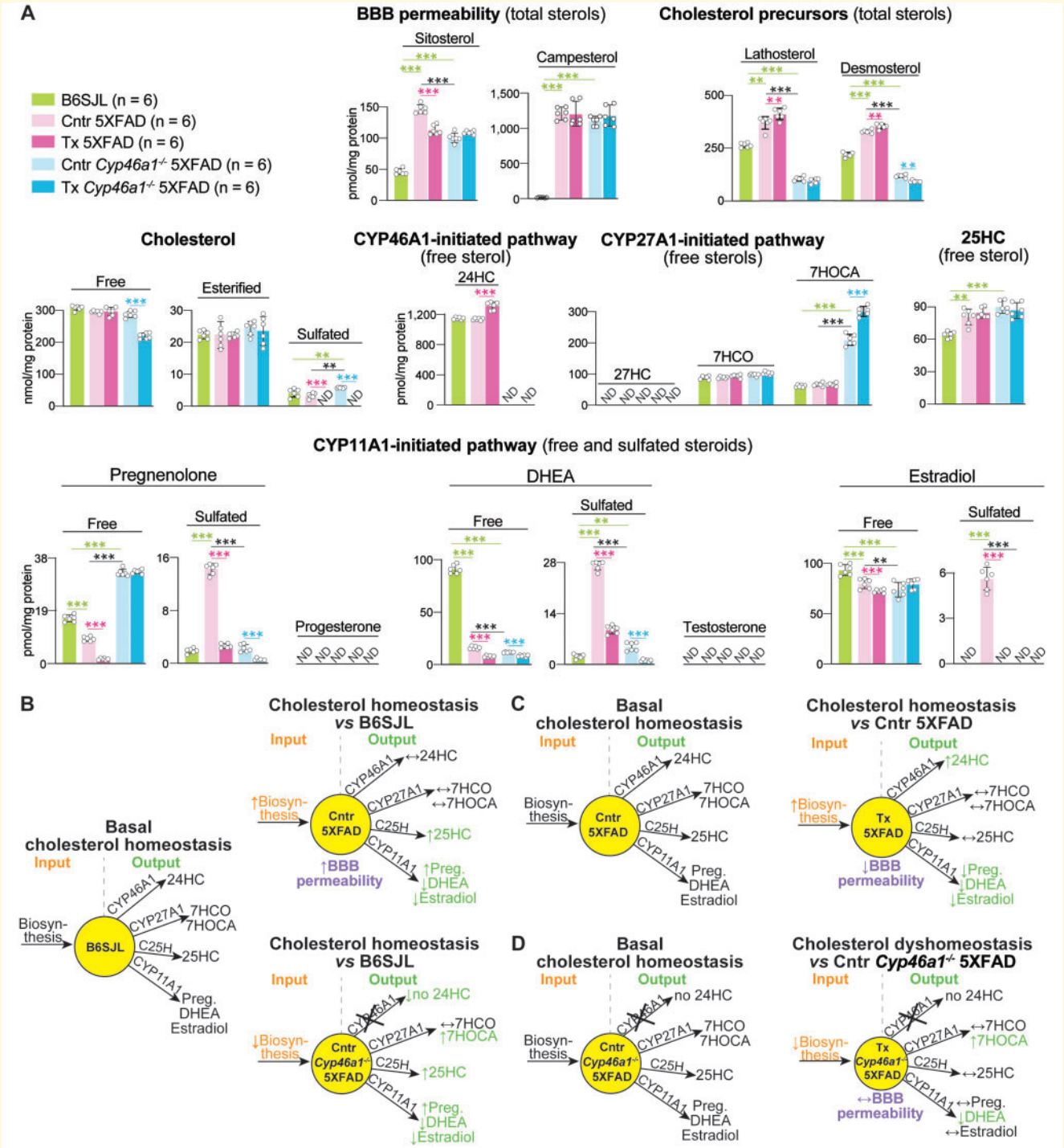

Figure 2 Brain sterols and steroids. (**A**) Absolute levels of the measured compounds. The results are the mean ± SD of individual measurements of brain homogenates ($n = 6$ male mice per group). Statistical analysis: a two way ANOVA followed by Bonferroni *post hoc* comparisons. Green lines and asterisks indicate statistically significant differences between control 5XFAD or *Cyp46a1*$^{-/-}$5XFAD mice versus B6SJL mice. Black lines and asterisks indicate statistically significant differences between control 5XFAD and *Cyp46a1*$^{-/-}$5XFAD mice. Magenta lines and asterisks indicate statistically significant differences between EFV-treated versus control mice 5XFAD mice. Cyan lines and asterisks indicate statistically significant differences between EFV-treated versus control *Cyp46a1*$^{-/-}$5XFAD mice. *$P \leq 0.05$; **$P \leq 0.01$, ***$P \leq 0.001$. (**B**–**D**) Schematic summary of quantifications in (**A**). Each yellow circle represents a pool of total cholesterol and is proportional to the size of this pool in the animal group indicated in the middle. Upwards (↑), downwards (↓) and left-right (↔) arrows indicate increases, decreases and no change in sterol/steroid levels, respectively, as compared to B6SJL mice (**B**) or control group (**C, D**). 7HCO = 7α-hydroxy-4-cholestene-3-one; 7HOCA = 7α-hydroxy-3-oxo-4-cholestenoic acid; 24HC = 24-hydroxycholesterol; 25HC = 25-hydroxycholesterol; 27HC = 27-hydroxycholesterol; BBB = blood-brain barrier; C25H = cholesterol 25-hydroxylase; Cntr = control (vehicle-treated mice); DHEA = dehydroepiandrosterone; ND = not detectable (the limit of detection for 27-hydroxycholesterol is 2 pmol/mg protein and that for progesterone, testosterone and sulfated forms is 0.5 pmol/mg protein); Preg = pregnenolone; Tx = EFV-treated mice.

(Lutjohann *et al.*, 1996). Instead, there is a flux of 27-hydroxycholesterol as well 7α-hydroxy-4-cholestene-3-one, a liver cholesterol metabolite, from the systemic circulation to the brain, where the two sterols are further metabolized by CYP27A1 to 7α-hydroxy-3-oxo-4-cholestenoic acid (Heverin *et al.*, 2005; Meaney *et al.*, 2007) (Fig. 1). 27-Hydroxycholesterol was below the detection limit in all five animal groups but 7α-hydroxy-4-cholestene-3-one was quantifiable and present at the same levels in all animals including those treated by EFV (Fig. 2A). In contrast, 7α-hydroxy-3-oxo-4-cholestenoic acid was significantly increased in control *Cyp46a1*$^{-/-}$5XFAD versus B6SJL mice, and EFV treatment further increased this sterol levels. Apparently, lack of cholesterol 24-hydroxylation in control *Cyp46a1*$^{-/-}$5XFAD versus B6SJL mice upregulated the CYP27A1-mediated sterol hydroxylation (Fig. 2B), and EFV treatment further enhanced this pathway while simultaneously decreasing the rate of cholesterol biosynthesis in *Cyp46a1*$^{-/-}$5XFAD mice (Fig. 2D). This led to the uncoupling of cholesterol elimination and biosynthesis and thereby disruption of the brain cholesterol homeostasis in EFV-treated *Cyp46a1*$^{-/-}$5XFAD mice.

25-Hydroxycholesterol is generated by cholesterol 25-hydroxylase (Fig. 1) as well as some other enzymes including CYP27A1 and represents a quantitatively minor product of cholesterol elimination from the brain (Lund *et al.*, 1998; Diczfalusy, 2013). The 25-hydroxycholesterol levels were increased in all groups of transgenic mice and were not affected by EFV treatment (Fig. 2A). Thus, animals with increased cholesterol biosynthesis (control 5XFAD mice) or lacking cholesterol 24-hydroxylation (control *Cyp46a1*$^{-/-}$5XFAD mice) also had increased cholesterol 25-hydroxylation (Fig. 2B). Conversely, EFV-treated 5XFAD and *Cyp46a1*$^{-/-}$5XFAD mice, which had increases in cholesterol 24-hydroxylation and C27-hydroxylations, respectively, had their 25-hydroxycholesterol levels unchanged (Fig. 2C and D).

CYP11A1 converts cholesterol to pregnenolone (Fig. 1), the first step in the biosynthesis of all steroid hormones (glucocorticoids, mineralocorticoids and sex hormones), and a quantitatively minor pathway of cholesterol metabolism in the brain (Mellon and Griffin, 2002; Hojo and Kawato, 2018). In B6SJL mice, the majority of pregnenolone was in the form of free steroids with pregnenolone sulfate representing ∼10% of the total pregnenolone content (Fig. 2A). Notably, in control 5XFAD mice, the sulfated and total pregnenolone levels were increased as is the free pregnenolone content in control *Cyp46a1*$^{-/-}$5XFAD mice. EFV treatment reduced the levels of both free and sulfated pregnenolone in 5XFAD mice and only the levels of sulfated pregnenolone in *Cyp46a1*$^{-/-}$5XFAD mice without affecting their total pregnenolone content. Thus, control 5XFAD versus B6SJL mice had simultaneous increases in cholesterol biosynthesis, the levels of 25-hydroxycholesterol and pregnenolone but unchanged metabolism by CYP46A1 (Fig. 2B). EFV treatment further increased their cholesterol biosynthesis and the 24-hydroxycholesterol levels but reduced the pregnenolone production (Fig. 2C). Control *Cyp46a1*$^{-/-}$5XFAD versus B6SJ mice had a decreased cholesterol biosynthesis but the upregulation of the CYP27A1-, cholesterol 25-hydroxylase- and CYP11A1-dependent cholesterol metabolism (Fig. 2B). EFV treatment further decreased cholesterol biosynthesis and increased CYP27A1-mediated hydroxylation (Fig. 2C).

Progesterone and dehydroepiandrosterone (DHEA) are the metabolites of pregnenolone, which are further converted into corticosteroids and sex hormones (Fig. 1). We could not detect progesterone in any groups of our mice but were able to quantify DHEA (Fig. 2A). Both control 5XFAD and *Cyp46a1*$^{-/-}$5XFAD mice had a reduction in the free DHEA levels as compared to B6SJL mice, and EFV treatment further reduced the free steroid levels in both genotypes. As in the case of pregnenolone, the extent of DHEA sulfation was the smallest in B6SJL mice (2%) and the largest in control 5XFAD mice (63%) with EFV treatment reducing the content of both sulfated and total DHEA (Fig. 2A). Testosterone, the primary male sex hormone, was not detectable in any groups of tested mice, whereas oestradiol, the primary female sex hormone, was quantifiable and was mainly unesterified in all mice except control 5XFAD animals. As compared to B6SJL mice, the total oestradiol levels were unchanged in control 5XFAD mice but were decreased in control *Cyp46a1*$^{-/-}$5XFAD. EFV treatment reduced the levels of sulfated and free oestradiol in 5XFAD mice while not affecting the hormone levels in *Cyp46a1*$^{-/-}$5XFAD mice. Apparently, the 5XFAD genotype increased the extent of pregnenolone, DHEA and oestradiol sulfation, whereas CYP46A1 lack (the *Cyp46a1*$^{-/-}$5XFAD genotype) exerted an opposite effect.

Brain Aβ burden

The quantifications were carried out by ELISA on brain homogenates and by ThioS stains on brain cryosections. EFV treatment of *Cyp46a1*$^{-/-}$5XFAD mice did not seem to alter either their levels of soluble or insoluble Aβ40 and Aβ42 peptides (Fig. 3) or the number and area of the ThioS-positive plaques in the cortex and hippocampus (Fig. 4). For comparison, in EFV-treated 5XFAD mice, the levels of soluble or insoluble Aβ40 and Aβ42 peptides were also unchanged, yet the number and area of the ThioS-positive plaques was decreased by 17–20% (Petrov *et al.*, 2019a). In addition, the levels of soluble and insoluble Aβ40 peptides were higher in control and EFV-treated 5XFAD mice than the respective groups of *Cyp46a1*$^{-/-}$5XFAD mice, yet their total Aβ load was unchanged as the Aβ42 species are predominant in the 5XFAD genotype (Supplementary Table 3).

Brain protein expression

The levels of glial fibrillary acidic protein (a marker for astrocyte activation), ionized calcium-binding adaptor molecule 1 (Iba1, a marker for microglia activation) as well as six synaptic proteins (Munc13-1, PSD-95, gephyrin, synaptophysin, synapsin-1 and calbindin) were quantified in brain homogenates by western blot. These were the same eight proteins that were previously evaluated in 5XFAD mice from the two treatment paradigms (Petrov *et al.*, 2019*a*, *b*). The quantification of the basal protein expression in control *Cyp46a1*$^{-/-}$5XFAD versus 5XFAD mice (Fig. 5) revealed that the expression of five proteins was decreased from 1.4- to 1.5-fold (glial fibrillary acidic protein, gephyrin and synapsin-1) to non-detectable (Munc13-1 and PSD-95). Two proteins (synaptophysin and calbindin) were expressed at the same levels, and one protein (Iba1) had a 1.7-fold increase in expression. Thus, the astrocyte activation was decreased in the control *Cyp46a1*$^{-/-}$5XFAD versus 5XFAD brains, whereas the microglia activation was increased. In addition, both presynaptic (Munc13-1 and synapsin-1) and post-synaptic (PSD-95) proteins had decreases in expression in the control *Cyp46a1*$^{-/-}$5XFAD brains. EFV treatment of *Cyp46a1*$^{-/-}$5XFAD mice did not seem to change the expression of the tested proteins (Fig. 6A–H), which was in contrast to changes in protein expression of glial fibrillary acidic protein, Iba1, Munc13-1, PSD-95 and synapsin-1 in EFV-treated 5XFAD from the second treatment paradigm (Fig. 6I). These changes could thus depend on CYP46A1 and its activity increase.

Munc13-1 is essential for synaptic vesicle priming, and PSD-95 is abundant in post-synaptic density (Migaud *et al.*, 1998; Augustin *et al.*, 1999). Simultaneous profound decreases in the expression of these two proteins in control *Cyp46a1*$^{-/-}$5XFAD versus 5XFAD mice (Figs 5 and 6) prompted further studies. These were assessments by transmission electron microscopy of synaptic contacts in synaptosomal fractions isolated from three groups of mice: control 5XFAD, control *Cyp46a1*$^{-/-}$5XFAD mice and EFV-treated *Cyp46a1*$^{-/-}$5XFAD mice. The focus was on the glutamatergic or asymmetric type 1 synapses, where Munc13-1 and PSD-95 are expressed, which have axons with round or spherical vesicles, and the postsynaptic membrane bordered on the cytoplasmic side by a thick dense opacity (Colonnier, 1968). Overall, the appearance of asymmetric synapses from all three

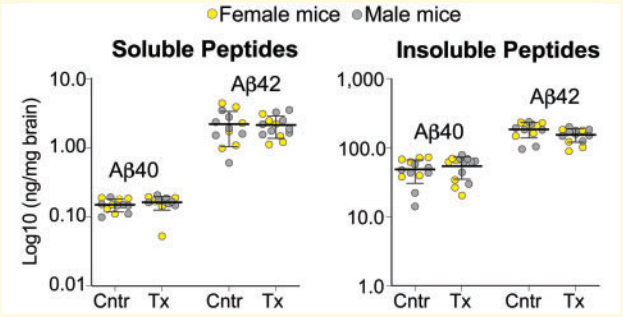

Figure 3 EFV effects on the amyloid β (Aβ) species in *Cyp46a1*$^{-/-}$5XFAD mice. The content of soluble and insoluble Aβ peptides was quantified by ELISA. The results are the mean ± SD of individual measurements of brain homogenates ($n = 6$ female and 7–8 male mice per group). Statistical analysis: mixed effects model followed by Bonferroni multiple comparisons. No significant differences were found between control (Cntr) and EFV-treated (Tx) mice when female and male mice were analysed as one group or separately.

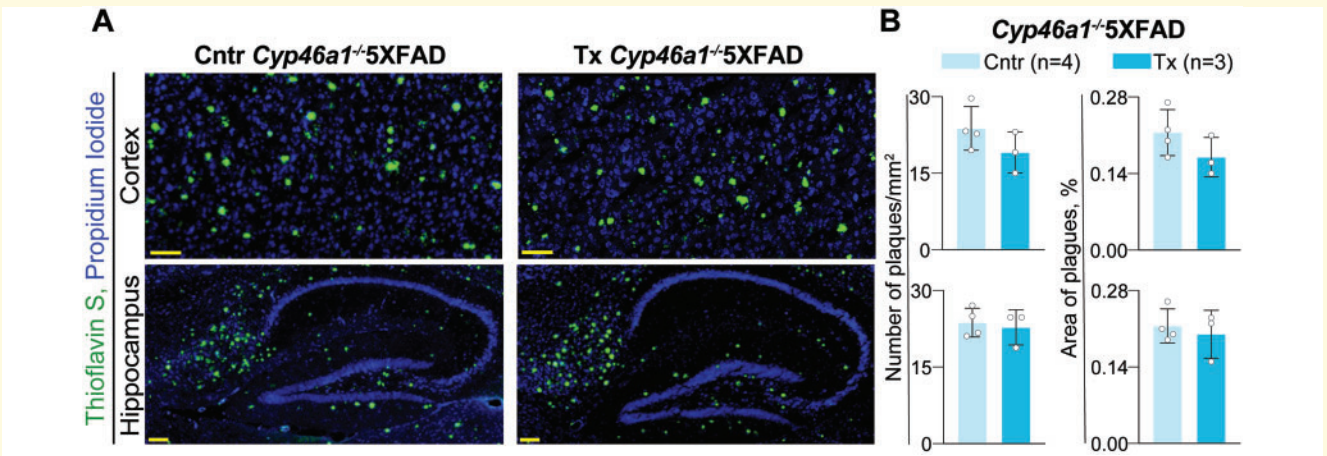

Figure 4 EFV effects on the number and area of the Thioflavin S-positive plaques. (**A**) Representative images of the stained brain sections from control (Cntr, 2 male and 2 female mice) and EFV-treated (Tx, 1 female and 2 male mice) groups; nuclei were stained with propidium iodide and falsely coloured in blue. (**B**) Quantifications of the Thioflavin S-positive plaques. Area of plaques is expressed as a percentage from the total area of either cortex or hippocampus. Statistical analysis: an unpaired, two-tailed Student's test. No significant differences were found between Cntr and EFV-treated Tx groups. Scale bars, 100 μM.

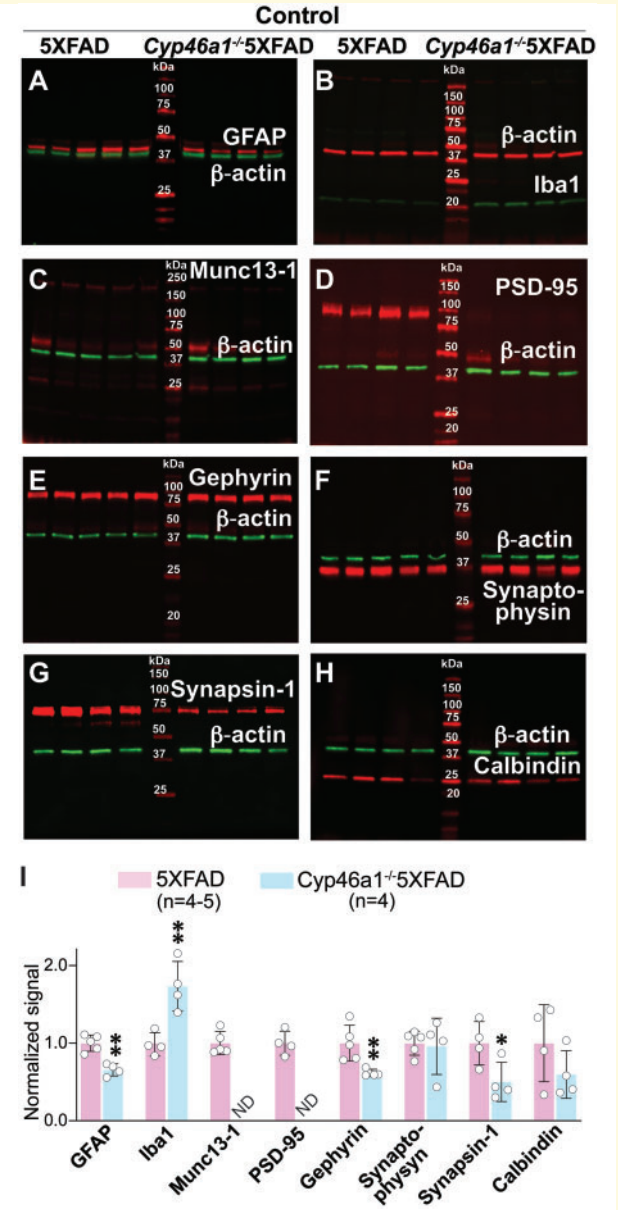

Figure 5 Brain expression of synaptic proteins in control mice. (**A–H**) Representative western blots ($n = 4$–5 male mice per group) of brain homogenates from 5XFAD and *Cyp46a1*$^{-/-}$5XFAD male mice. Each lane, except those with molecular weight markers, represents a sample from an individual animal. (**I**) Quantification of the relative protein expression in (**A–H**). Protein expression in each sample within a group was first normalized to the β-actin expression followed by the calculation of the mean value of the protein expression within a group. This mean value was then normalized to the mean value of the protein expression in control 5XFAD mice, which was taken as one. The results the mean ± SD of the measurements in individual mice. Statistical analysis: a two-tailed, unpaired Student's test. *$P \leq 0.05$; **$P \leq 00.1$.

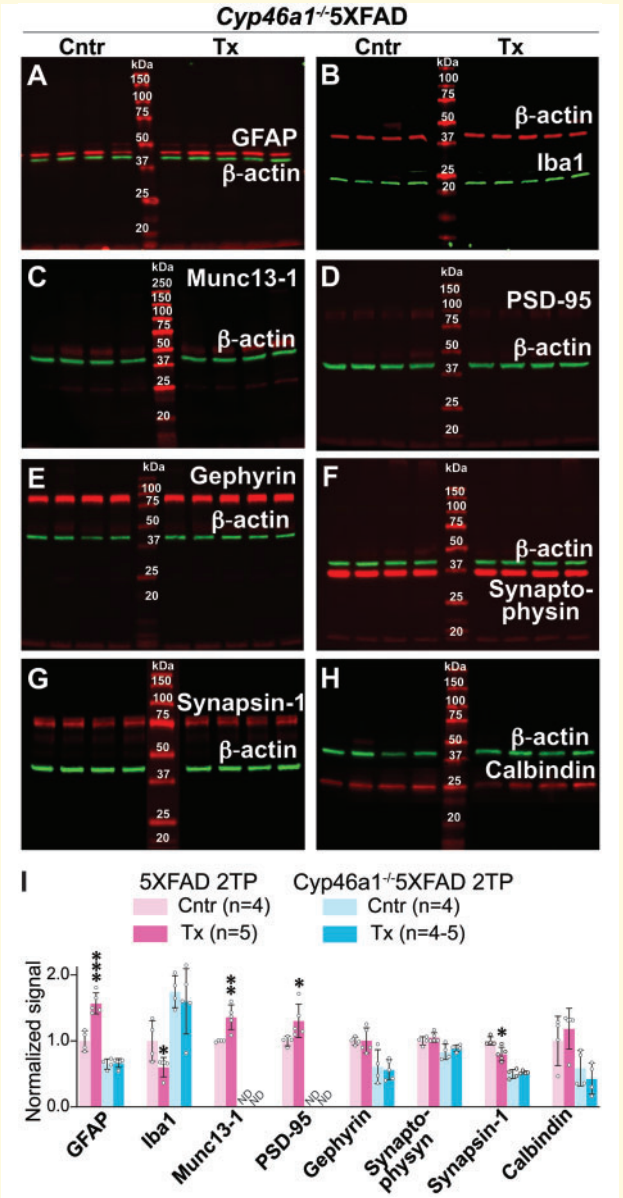

Figure 6 EFV effects on brain expression of synaptic proteins in *Cyp46a1*$^{-/-}$5XFAD mice. (**A–H**) Representative western blots ($n = 4$–5 per group) of brain homogenates from control (Cntr) and EFV-treated (Tx) *Cyp46a1*$^{-/-}$5XFAD male mice. Each lane, except those with molecular weight markers, represents a sample from individual animal. (**I**) A comparison of the relative protein expression in EFV-treated versus control mice of different genotypes. Data for 5XFAD mice from the second treatment paradigm (2TP) are taken from Petrov *et al.* (2019a) and those for *Cyp46a1*$^{-/-}$5XFAD mice represent the quantifications of protein expression in (**A–H**) as described in Fig. 5. Statistical analysis: a two-tailed, unpaired Student's test. *$P \leq 0.05$; **$P \leq 00.1$, ***$P \leq 0.001$.

groups of mice seemed to be similar with docked vesicles on the presynaptic membrane and patches of a thick opacity fused to the post-synaptic membrane (Supplementary Fig. 1). This result is consistent with morphologically normal synapses in *Munc13-1*$^{-/-}$ mice, most of which are, however, incapable of neurotransmission (Augustin *et al.*, 1999), and unaffected morphology of synapses in

Psd-95$^{-/-}$ mice, which, nevertheless, have impaired learning (Migaud *et al.*, 1998).

Brain gene expression

RNA-Seq and qRT-PCR of brain homogenates were used. RNA-Seq detected 19 907 and 18 273 genes in the brain of 5XFAD and *Cyp46a1*$^{-/-}$5XFAD mice, respectively (Supplementary Fig. 2). Of them, 173 genes in 5XFAD mice and 189 genes in *Cyp46a1*$^{-/-}$5XFAD mice had at least a 2.0-fold difference in expression (an arbitrary cut off) between EFV-treated and control groups and q of ≤ 0.05 (Supplementary Tables 4 and 5). In EFV-treated versus control 5XFAD mice, 71 and 102 of the differentially expressed genes were upregulated and downregulated, respectively. In EFV-treated versus control *Cyp46a1*$^{-/-}$5XFAD mice, increased and decreased expression was found for 46 and 143 genes, respectively. Overall, genes affected by EFV treatment did not overlap in 5XFAD and *Cyp46a1*$^{-/-}$5XFAD mice except *Pdcd1lg2*, *Becn2*, *Podnl1* and *Fam83c* (Supplementary Fig. 2). *Pdcd1lg2* was upregulated and *Becn2* was downregulated in both genotypes, whereas *Podnl1* and *Fam83c* had opposite changes in expression in EFV-treated 5XFAD or *Cyp46a1*$^{-/-}$5XFAD mice versus their respective controls.

A total of 82 genes were then quantified by qRT-PCR. They included 63 genes which had altered expression in RNA-Seq either in EFV-treated versus control 5XFAD mice, EFV-treated versus control *Cyp46a1*$^{-/-}$5XFAD mice or both (Supplementary Tables 4 and 5). Plus 19 genes were selected additionally by us based on the results of steroid quantifications (Fig. 2) and the reported EFV effects on the vitamin D_3 metabolism (Supplementary Fig. 3). Changes in the expression of the latter 19 genes were not statistically significant in RNA-Seq. The measurements by qRT-PCR documented altered expression of 48 from 63 genes indicated by RNA-Seq and 18 of 19 genes selected by us (Figs 7 and 8). Next, the directionality of changes in EFV-treated 5XFAD and *Cyp46a1*$^{-/-}$5XFAD mice versus their corresponding controls was compared to identify *Cyp46a1*-dependent and independent effects; the algorithm for this determination is shown in Fig. 7A. The *Cyp46a1*-dependent changes were observed for more than a half of the genes from the neuroprotection, neurogenesis, synaptic function, and apoptosis groups (Figs 7B and 8). The *Cyp46a1*-independent changes were found for all of the tested genes in the cholinergic neurotransmission group and for more than a half of the genes in the groups pertaining to monoaminergic and peptidergic neurotransmission, homeostasis of sulfated steroids, steroidogenesis, vitamin D_3 and other genes (Figs 7B and 8). In addition, an about equal split between *Cyp46a1*-independent and depended changes in the gene expression in EFV-treated mice of both genotypes was documented for the inflammation and immune response group. Overall, of the 82 genes quantified by qRT-PCR, 49 and 26 had changes in the expression as a result of EFV treatment independent and dependent of CYP46A1, respectively, and 5 genes had either unchanged or undetectable expression. This statistics suggested that EFV could act as a transcriptional modulator.

Discussion

Herein, we continued to investigate the CYP46A1 role in the brain and contribution to EFV treatment effects. By using brain homogenates, we studied the CYP46A1 significance at the whole organ level, yet have to acknowledge that lack of changes in brain homogenates does not exclude changes in specific cell populations which could remain undetected. Our sterol and steroid characterizations revealed a tight coupling between cholesterol biosynthesis and cholesterol metabolism not only by CYP46A1 but also by CYP27A1, cholesterol 25-hydroxylase and CYP11A1, the other cholesterol hydroxylating enzymes (Fig. 2B–D). Normally, the three hydroxylases utilize only little of brain cholesterol but their activities are important as they generate biologically active molecules (Janowski *et al.*, 1999). Hence, uncovering that the activity of all four cholesterol hydroxylases in the brain is tightly coordinated provides mechanistic insight into how the brain levels of some of the biologically active endogenous compounds (e.g. 25-hydroxycholesterol, DHEA and progesterone) could be regulated.

We linked cholesterol metabolism by CYP46A1 to the pregnenolone production by CYP11A1 (Fig. 2C) and hence steroidogenesis as pregnenolone formation is a rate-limiting step in the biosynthesis of all steroid hormones (Stone and Hechter, 1954). We also documented that the total pregnenolone levels (Fig. 2A) did not always correlate with the *Cyp11a1* basal expression in control 5XFAD and *Cyp46a1*$^{-/-}$5XFAD mice versus B6SJL mice (Fig. 8). Similarly, there was no clear correlation between increased *Cyp11a1* expression in EFV-treated versus control mice of both genotypes and their pregnenolone production. In the adrenals, the rate-limiting factor for pregnenolone production is cholesterol delivery to the inner mitochondrial membrane where CYP11A1 resides, whereas in the placenta, this factor is electron delivery to CYP11A1 (Crivello and Jefcoate, 1980; Tuckey, 2005). Our data (Fig. 2B–D) suggest that cholesterol availability for steroidogenesis could be a post-translational regulator of pregnenolone production in the brain.

The EFV effect on the levels of DHEA and oestradiol (Fig. 2A) is another important finding as steroid hormones, including DHEA, are tested as brain therapeutics due to involvement in a myriad of brain functions by acting as allosteric modulators of neurotransmitter receptors, ligands for specific steroid receptors and non-genomic regulators (Baulieu, 1997; Porcu *et al.*, 2016; Diotel *et al.*, 2018; Murakami *et al.*, 2018). Yet, brain delivery of neuroactive steroids as pharmacologic agents is

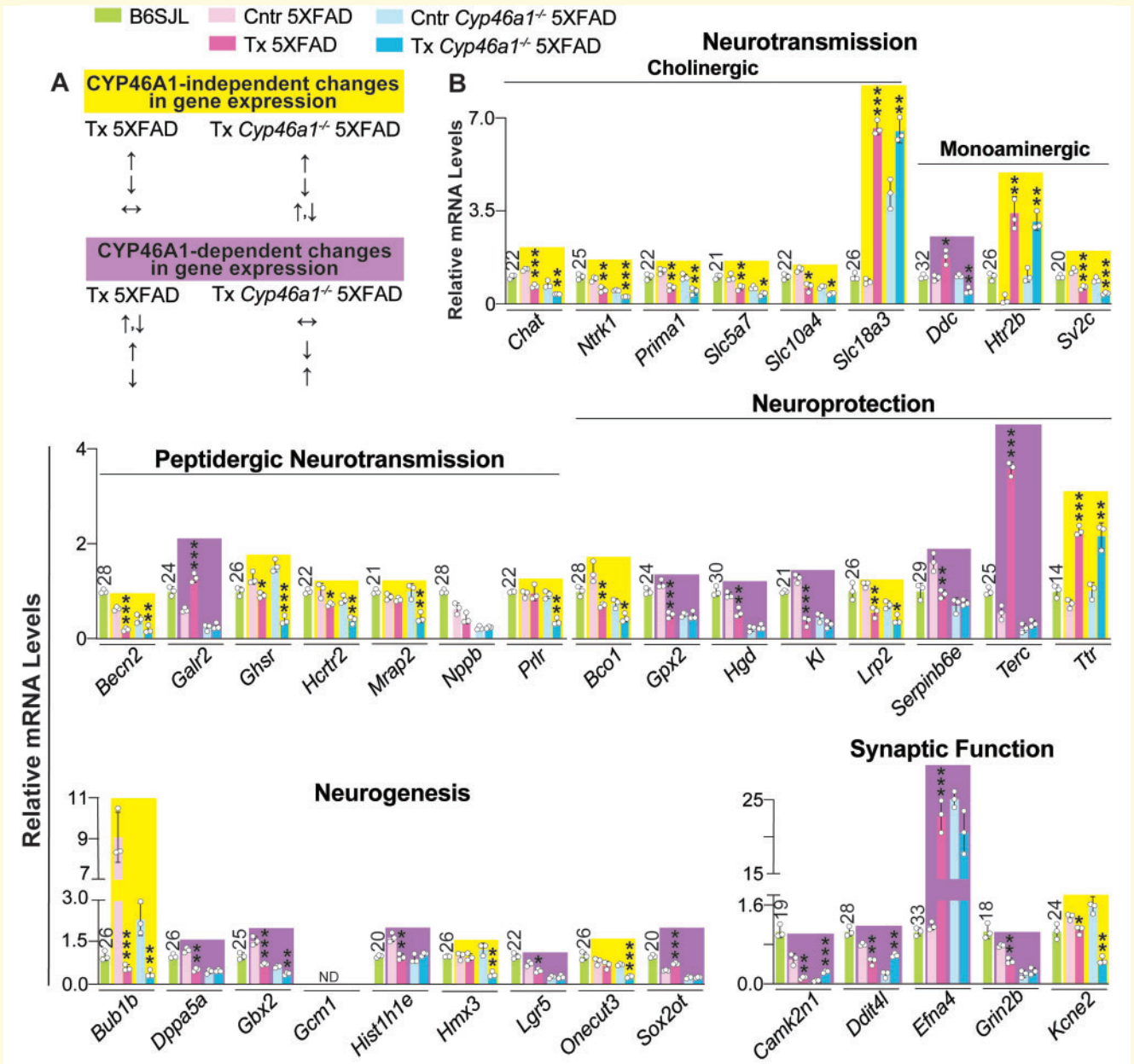

Figure 7 EFV effects on brain expression of genes related to neurons. Gene symbols are as designated in the National Center for Biotechnology Information's gene database. (**A**) The algorithm for determination of CYP46A1-independent (yellow box) and dependent (violet box) EFV effects. Upwards (↑), downwards (↓) and left-right (↔) arrows indicate increases, decreases and no change in gene expression, respectively, as compared to the corresponding control group. (**B**) Relative gene expression as assessed by qRT-PCR. The results are the mean ± SD of individual measurements of brain homogenates ($n = 3$ male mice per group). Each gene expression was first normalized to the *Gapdh* expression and then averaged. This mean value was then normalized to the mean value of the gene expression in BSJL mice, which was taken as one. Statistical analysis: an unpaired, two-tailed Student's test. *$P \leq 0.05$; **$P \leq 00.1$, ***$P \leq 0.001$ versus the corresponding control group. The Ct numbers for the B6SJL strain are indicated above bars. Cntr = control (vehicle-treated mice); Tx = EFV-treated mice.

challenging due to systemic effects, low bioavailability for the brain and potential for addiction in addition to safety and tolerability issues (Porcu *et al.*, 2016). Hence, modulation of brain steroidogenesis *in situ* by EFV treatment could be a novel therapeutic option for treatment of at least some of the pathologic conditions in the brain (Goncharov and Katsya, 2013; Tang *et al.*, 2015).

We documented that similar to EFV-treated versus control 5XFAD mice (Petrov *et al.*, 2019a), EFV-treated versus control *Cyp46a1*$^{-/-}$5XFAD mice did not have a change in the levels of the individual Aβ species as assessed by ELISA (Fig. 3). Yet, the absolute levels of the Aβ40 peptides were decreased in the *Cyp46a1*$^{-/-}$5XFAD versus 5XFAD genotype (Supplementary Table 3).

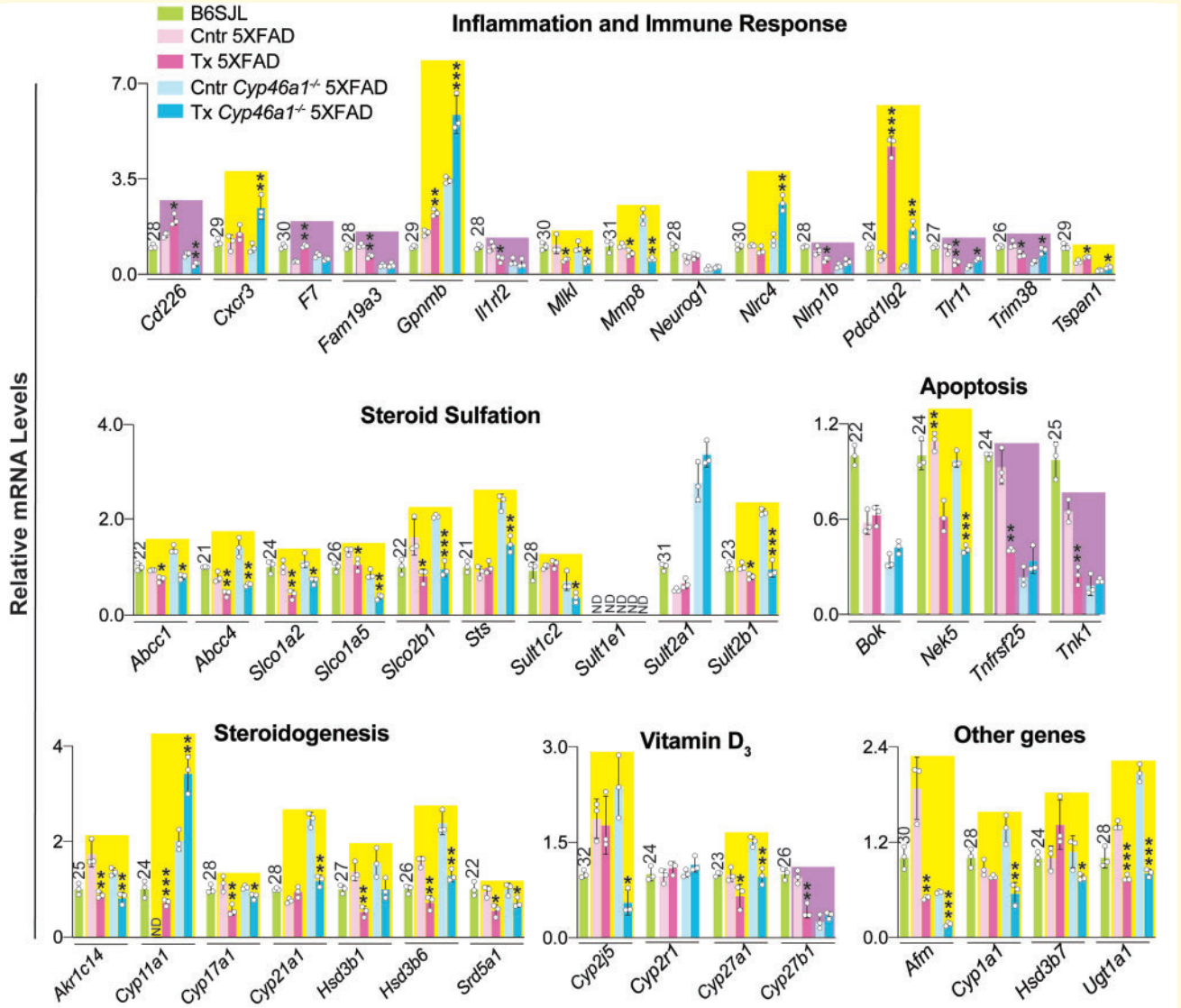

Figure 8 EFV effects on brain expression of genes related to general biological processes. Relative gene expression in brain homogenates as assessed by qRT-PCR. The results are the mean ± SD of individual measurements ($n = 3$ male mice per group). The normalization of gene expression and box colour code are as in Fig. 7. Statistical analysis: an unpaired, two-tailed Student's test. $^{*}P \leq 0.05$; $^{**}P \leq 00.1$, $^{***}P \leq 0.001$ versus the corresponding control group. The Ct numbers for the B6SJL strain are indicated above bars. Cntr = control (vehicle-treated mice); Tx = EFV-treated mice.

Furthermore, EFV-treated versus control *Cyp46a1*$^{-/-}$5XFAD mice did not have a change in the number and area of the ThioS-positive plaques in the cortex and hippocampus (Fig. 4). In contrast, EFV-treated versus control 5XFAD mice had such a decrease (Petrov *et al.*, 2019a). Thus, there seem to be links between CYP46A1 and the Aβ burden.

The present study found that in control *Cyp46a1*$^{-/-}$5XFAD versus 5XFAD mice (Fig. 5), there was a profound decrease in the expression of Munc13-1, an important pre-synaptic protein (Augustin *et al.*, 1999), and PSD-95, the major scaffolding protein in the excitatory postsynaptic density (Migaud *et al.*, 1998). When combined with increases in the Munc13-1 and PSD-95 expression in EFV-treated versus control 5XFAD mice (Fig. 6I), this result is consistent with the CYP46A1-dependent mechanism of expression changes, possibly *via* the effect on protein phosphorylation (Petrov *et al.*, 2020). Indeed, loss of PSD-95 from dendritic spines was shown to depend on its phosphorylation by calcium/calmodulin-dependent protein kinase II (CAMKII) and glycogen synthase kinase 3β (GSK3β) (Steiner *et al.*, 2008; Nelson *et al.*, 2013; Patriarchi *et al.*, 2018). In turn, CAMKII activity could be altered by calcium/calmodulin-dependent protein kinase II inhibitor 1 (CAMK2N1), whose gene expression was altered upon EFV treatment (under synaptic function, Fig. 7B). The GSK3 activity could also be changed by EFV as drug

treatment of 5XFAD mice (or increased sterol flux through the plasma membranes) was shown to abolish GSK3β engagement in KCl-induced glutamate exocytosis in synaptosomal fractions isolated from the brain of these animals (Petrov *et al.*, 2020). Consequently, lack of CYP46A1 (or decreased sterol flux) could affect GSK3β activity as well and thereby PSD-95 phosphorylation and protein content. Further studies are required to ascertain the interplay between CYP46A1, CAMKII and GSK3β activities and expression of PSD-95 and Munc13-1.

EFV-treated 5XFAD mice from the first treatment paradigm had drug effects on multiple processes including those that relate to inflammation, oxidative stress and apoptosis (Petrov *et al.*, 2019b). Herein, the *Cyp46a1*-dependent EFV effects also included those on the expression of genes pertaining to inflammation (*Cd226*, *F7*, *Fam19a3*, *Il1rl2*, *Nlrp1b*, *Tlr11* and *Trim38*), oxidative stress (e.g. *Terc and Gpx2*, placed in neuroprotection) and apoptosis (*Tnfrsf25* and *Tnk1*) (Figs 7B and 8). In control *Cyp46a1*$^{-/-}$5XFAD versus 5XFAD mice, CYP46A1 absence affected the basal glial fibrillary acidic protein and Iba1 expression, i.e. astrocyte and microglia activation, and eliminated the effect of EFV treatment (Figs 5I and 6I). Accordingly, changes in astrocyte and microglia activation in control *Cyp46a1*$^{-/-}$5XFAD versus 5XFAD mice can explain in part the modulation of the basal expression of some of their inflammatory and immune response genes (Fig. 8) as well as gene response to efavirenz treatment. Further studies are required to support this inference.

New groups of genes affected by CYP46A1 activity increases were identified: those involved in neuroprotection (*Hgd*, *Kl and Serpinb6e*), neurogenesis (*Dppa5a*, *Gbx2*, *Hist1h1e*, *Lgr5* and *Sox2ot*), and synaptic function (*Camk2n1*, *Ddit4l*, *Efna4*, *Grin2b, Ddc* and *Galr2*, the latter two are under monoaminergic and peptidergic neurotransmission, respectively, Fig. 7B). Of these newly identified genes, three (*Terc*, *Camk2n1* and *Efna4*) are worth further discussion because of their broad biological importance and the magnitude of expression changes upon EFV treatment. *Terc* (telomerase RNA component, under neuroprotection, Fig. 7B) is a ribonucleoprotein responsible for the maintenance of telomere length and thereby genome stability and cellular life span (González-Giraldo *et al.*, 2016). A 6.6-fold upregulation of *Terc* in EFV-treated versus control 5XFAD mice and its unchanged expression in EFV-treated versus control *Cyp46a1*$^{-/-}$5XFAD (Fig. 7B) suggest that this EFV effect is likely protective in 5XFAD mice as it may restore the telomer lengths (Mitchell *et al.*, 1999; Eitan *et al.*, 2014; Eitan *et al.*, 2016).

Camk2n1 (under synaptic function, Fig. 7B) inhibits CAMKII, a key synaptic signalling molecule for learning and memory, which was suggested to keep synapses in an operative range allowing further potentiation (Gouet *et al.*, 2012). A reduced *Camk2n1* expression was shown to not significantly affect contextual fear long-term memory formation, whereas an increased expression was found to impair contextual fear long-term memory formation but not its maintenance (Vigil *et al.*, 2017). Previously, we found that EFV treatment improved the short- and long-term contextual fear memory in 5XFAD mice (Petrov *et al.*, 2019a). Accordingly, a 5-fold decrease and a 4.2-fold increase in the *Camk2n1* levels in EFV-treated 5XFAD and *Cyp46a1*$^{-/-}$5XFAD mice, respectively (Fig. 7B) could represent positive and negative EFV effects.

Efna4 (under synaptic function, Fig. 7B) encodes the tyrosine kinase ephrin receptor A4, which is essential for synaptic function as it mediates dendritic spine morphogenesis, synapse formation, and maturation (Murai *et al.*, 2003). A 20-fold *Efna4* upregulation in EFV-treated 5XFAD mice (Fig. 7B) could increase receptor availability and therefore represent a positive effect of drug treatment (Murai *et al.*, 2003; Chen *et al.*, 2012; Rosenberger *et al.*, 2014), which, however, is not observed in EFV-treated *Cyp46a1*$^{-/-}$5XFAD mice.

Of the CYP46A1-independent EFV effects, the majority was on the cholinergic, monoaminergic and peptidergic neurotransmission with all of the key genes involved in cholinergic neurotransmission being affected by EFV treatment (Fig. 7B). Overall, EFV treatment downregulated the expression of all studied cholinergic and monoaminergic neurotransmission genes, except *Slc18a3* and *Htr2b* which were upregulated. The downregulation was moderate (up to 2-fold) in both 5XFAD and *Cyp46a1*$^{-/-}$5XFAD mice, whereas the upregulation was more significant, especially in EFV-treated 5XFAD mice (8- or 23-fold). At a 600 mg/day dose given to humans, many of the EFV adverse effects are similar to those elicited by lysergic acid diethylamine (Gatch *et al.*, 2013; Dalwadi *et al.*, 2016; Dalwadi *et al.*, 2018). Therefore, multiple receptors (serotonin—5-HT$_{2A,2B,2C,3A,6}$; γ-aminobutyric acid—GABA$_A$; and muscarinic—M$_{1,3}$) as well as transporters (dopamine and serotonin along with vesicular monoamine transporter 2) and monoamine oxidase A were identified, which can bind EFV and contribute to the drug's adverse effects (Gatch *et al.*, 2013; Dalwadi *et al.*, 2016). EFV doses which elicit the lysergic acid-like effects in mice (>10 mg/kg body weight) are much higher than the 0.1 mg/kg body weight dose used in the present study. Also, we did not observe head twitching in EFV-treated mice, a common mouse behavioural proxy of hallucinations in humans (Gatch *et al.*, 2013). Thus, it not clear whether the moderate EFV effects on the expression of the neurotransmission genes in 5XFAD and *Cyp46a1*$^{-/-}$5XFAD mice indeed altered different types of neurotransmission.

The CYP46A1-independent EFV effects on the expression of steroidogenic genes (Fig. 8) were unexpected but could be explained in retrospect by the coordinated transcription of steroidogenesis (Sewer and Waterman, 2003; Miller and Bose, 2011) with EFV acting as a common

transcriptional regulator. To the best of our knowledge, steroid sulfation has not yet been studied in the brain of 5XFAD mice, and we discovered that more than a half of the brain pregnenolone and DHEA were sulfated in this genotype (Fig. 2). This result prompted the qRT-PCR quantifications of the genes involved in steroid sulfation as well as the genes of vitamin D_3 metabolism (Supplementary Fig. 3). Vitamin D_3 was shown to regulate the expression of different sulfotransferases as well as some of the steroidogenic genes and proteins in cell culture (Dubaisi *et al.*, 2018; Emanuelsson *et al.*, 2018). In addition, the sulfotransferase expression was shown to be regulated by constitutive androstane receptor (CAR) and pregnane X receptor (PXR), which could be activated by EFV (Faucette *et al.*, 2007; Sharma *et al.*, 2013; Narayanan *et al.*, 2018) (Supplementary Fig. 3). Indeed, the expression of all of the sulfation-related genes was altered (except *Cyp27b1* under vitamin D_3, Fig. 8) and consistent with EFV being a transcriptional regulator in the 5XFAD and *Cyp46a1*$^{-/-}$5XFAD brain for at least some of these genes despite of a very small dose used. The transcription factors mediating the EFV effect on gene expression and ultimately steroid sulfation in the brain remain to be determined.

In conclusion, we generated *Cyp46a1*$^{-/-}$5XFAD mice and compared the EFV treatment effects on the brain of these and 5XFAD animals. We revealed the details of the brain cholesterol biosynthesis-cholesterol metabolism link and discovered that in the 5XFAD brain, CYP46A1 activity regulates the production of pregnenolone, likely by affecting cholesterol availability to CYP11A1, which converts cholesterol to pregnenolone. Additional CYP46A1-dependent EFV effects included changes in the brain levels of such synaptic proteins as Munc13-1, PSD-95, gephyrin, synaptophysin and synapsin-1 along with the markers of astrocyte (glial fibrillary acidic protein) and microglia (Iba1) activation. The change in the PSD-95 expression was consistent with the effect of the CYP46A1-dependent sterol flux on the protein phosphorylation by CAMII (possibly *via* CAMK2N1) and GSK3β. The CYP46A1-independent changes mainly included EFV effects on gene expression, thus suggesting that EFV acts as a transcriptional regulator even at a small dose used. Yet, it is not clear whether the gene transcription changes were translated into protein expression changes and ultimately reflected in functionality. This study further confirms that CYP46A1 is a key regulator of cholesterol homeostasis in the brain and that the favourable EFV effects on behavioural performance of 5XFAD mice are realized *via* the CYP46A1-dependent mechanism.

Supplementary material

Supplementary material is available at *Brain Communications* online.

Acknowledgements

The authors thank the Case Western Reserve University Visual Sciences Research Center Core Facilities for assistance with mouse breeding (Heather Butler) and genotyping (John Denker). The authors are also grateful to Dr. Hisashi Fujioka (Electron Microscopy Core facility) for help with studies of synaptosomal ultrastructure.

Funding

This work was supported in part in by the U.S. National Institute of Health Grants AG067552 and EY011373 (to I.A.P.).

Competing interests

The authors report no competing interests. We confirm that we have read the Journal's position on issues involved in ethical publication and affirm that this report is consistent with those guidelines.

References

Apostolova N, Blas-Garcia A, Galindo MJ, Esplugues JV. Efavirenz: what is known about the cellular mechanisms responsible for its adverse effects. Eur J Pharmacol 2017; 812: 163–73.

Apostolova N, Funes HA, Blas-Garcia A, Galindo MJ, Alvarez A, Esplugues JV. Efavirenz and the CNS: what we already know and questions that need to be answered. J Antimicrob Chemother 2015; 70: 2693–708.

Augustin I, Rosenmund C, Südhof TC, Brose N. Munc13-1 is essential for fusion competence of glutamatergic synaptic vesicles. Nature 1999; 400: 457–61.

Bankhead P, Loughrey MB, Fernández JA, Dombrowski Y, McArt DG, Dunne PD, et al. QuPath: Open source software for digital pathology image analysis. Sci Rep 2017; 7: 16878.

Baulieu EE. Neurosteroids: of the nervous system, by the nervous system, for the nervous system. Recent Prog Horm Res 1997; 52: 1–32.

Bjorkhem I, Lutjohann D, Diczfalusy U, Stahle L, Ahlborg G, Wahren J. Cholesterol homeostasis in human brain: turnover of 24S-hydroxycholesterol and evidence for a cerebral origin of most of this oxysterol in the circulation. J Lipid Res 1998; 39: 1594–600.

Björkhem I, Meaney S. Brain cholesterol: long secret life behind a barrier. Arterioscler Thromb Vasc Biol 2004; 24: 806–15.

Boussicault L, Alves S, Lamazière A, Planques A, Heck N, Moumné L, et al. CYP46A1, the rate-limiting enzyme for cholesterol degradation, is neuroprotective in Huntington's disease. Brain 2016; 139: 953–70.

Brown J, Theisler C, Silberman S, Magnuson D, Gottardi-Littell N, Lee JM, et al. Differential expression of cholesterol hydroxylases in Alzheimer's disease. J Biol Chem 2004; 279: 34674–81.

Burlot M-A, Braudeau J, Michaelsen-Preusse K, Potier B, Ayciriex S, Varin J, et al. Cholesterol 24-hydroxylase defect is implicated in memory impairments associated with Alzheimer-like Tau pathology. Hum Mol Genet 2015; 24: 5965–76.

Cartagena CM, Ahmed F, Burns MP, Pajoohesh-Ganji A, Pak DT, Faden AI, et al. Cortical injury increases cholesterol 24S hydroxylase (Cyp46) levels in the rat brain. J Neurotrauma 2008; 25: 1087–98.

Chen Y, Fu AKY, Ip NY. Eph receptors at synapses: implications in neurodegenerative diseases. Cell Signal 2012; 24: 606–11.

Colonnier M. Synaptic patterns on different cell types in the different laminae of the cat visual cortex. An electron microscope study. Brain Res 1968; 9: 268–87.

Crivello JF, Jefcoate CR. Intracellular movement of cholesterol in rat adrenal cells. Kinetics and effects of inhibitors. J Biol Chem 1980; 255: 8144–51.

Dalwadi DA, Kim S, Amdani SM, Chen Z, Huang R-Q, Schetz JA. Molecular mechanisms of serotonergic action of the HIV-1 antiretroviral efavirenz. Pharmacol Res 2016; 110: 10–24.

Dalwadi DA, Ozuna L, Harvey BH, Viljoen M, Schetz JA. Adverse neuropsychiatric events and recreational use of efavirenz and other HIV-1 antiretroviral drugs. Pharmacol Rev 2018; 70: 684–711.

Diczfalusy U. On the formation and possible biological role of 25-hydroxycholesterol. Biochimie 2013; 95: 455–60.

Diotel N, Charlier TD, Lefebvre d'Hellencourt C, Couret D, Trudeau VL, Nicolau JC, et al. Steroid transport, local synthesis, and signaling within the brain: roles in neurogenesis, neuroprotection, and sexual behaviors. Front Neurosci 2018; 12: 84.

Dubaisi S, Barrett KG, Fang H, Guzman-Lepe J, Soto-Gutierrez A, Kocarek TA, et al. Regulation of cytosolic sulfotransferases in models of human hepatocyte development. Drug Metab Dispos 2018; 46: 1146–56.

Eitan E, Hutchison ER, Mattson MP. Telomere shortening in neurological disorders: an abundance of unanswered questions. Trends Neurosci 2014; 37: 256–63.

Eitan E, Tamar A, Yossi G, Peleg R, Braiman A, Priel E. Expression of functional alternative telomerase RNA component gene in mouse brain and in motor neurons cells protects from oxidative stress. Oncotarget 2016; 7: 78297–309.

Emanuelsson I, Almokhtar M, Wikvall K, Grönbladh A, Nylander E, Svensson A-L, et al. Expression and regulation of CYP17A1 and 3beta-hydroxysteroid dehydrogenase in cells of the nervous system: Potential effects of vitamin D on brain steroidogenesis. Neurochem Int 2018; 113: 46–55.

Faucette SR, Zhang T-C, Moore R, Sueyoshi T, Omiecinski CJ, LeCluyse EL, et al. Relative activation of human pregnane X receptor versus constitutive androstane receptor defines distinct classes of CYP2B6 and CYP3A4 inducers. J Pharmacol Exp Ther 2007; 320: 72–80.

Gatch MB, Kozlenkov A, Huang R-Q, Yang W, Nguyen JD, González-Maeso J, et al. The HIV antiretroviral drug efavirenz has LSD-like properties. Neuropsychopharmacology 2013; 38: 2373–84.

Goncharov NP, Katsya GV. Neurosteroid dehydroepiandrosterone and brain function. Hum Physiol 2013; 39: 667–74.

González-Giraldo Y, Forero DA, Echeverria V, Gonzalez J, Ávila-Rodriguez M, Garcia-Segura LM, et al. Neuroprotective effects of the catalytic subunit of telomerase: a potential therapeutic target in the central nervous system. Ageing Res Rev 2016; 28: 37–45.

Gouet C, Aburto B, Vergara C, Sanhueza M. On the mechanism of synaptic depression induced by CaMKIIN, an endogenous inhibitor of CaMKII. PLoS One 2012; 7: e49293.

Halford RW, Russell DW. Reduction of cholesterol synthesis in the mouse brain does not affect amyloid formation in Alzheimer's disease, but does extend lifespan. Proc Natl Acad Sci USA 2009; 106: 3502–6.

Han M, Wang S, Yang N, Wang X, Zhao W, Saed HS. Therapeutic implications of altered cholesterol homeostasis mediated by loss of CYP46A1 in human glioblastoma. EMBO Mol Med 2019; e10924.

Heverin M, Meaney S, Lütjohann D, Diczfalusy U, Wahren J, Björkhem I. Crossing the barrier: net flux of 27-hydroxycholesterol into the human brain. J Lipid Res 2005; 46: 1047–52.

Hojo Y, Kawato S. Neurosteroids in adult hippocampus of male and female rodents: biosynthesis and actions of sex steroids. Front Endocrinol (Lausanne) 2018; 9: 183.

Hudry E, Van Dam D, Kulik W, De Deyn PP, Stet FS, Ahouansou O, et al. Adeno-associated virus gene therapy with cholesterol 24-hydroxylase reduces the amyloid pathology before or after the onset of amyloid plaques in mouse models of Alzheimer's disease. Mol Ther 2010; 18: 44–53.

Janowski BA, Grogan MJ, Jones SA, Wisely GB, Kliewer SA, Corey EJ, et al. Structural requirements of ligands for the oxysterol liver X receptors LXRalpha and LXRbeta. Proc Natl Acad Sci USA 1999; 96: 266–71.

Jiang Z, Gu L, Liang X, Cao B, Zhang J, Guo X. The effect of selenium on CYP450 isoform activity and expression in pigs. Biol Trace Elem Res 2020; 196: 454–62.

Kacher R, Lamazière A, Heck N, Kappes V, Mounier C, Despres G, et al. CYP46A1 gene therapy deciphers the role of brain cholesterol metabolism in Huntington's disease. Brain 2019; 142: 2432–50.

Karu K, Hornshaw M, Woffendin G, Bodin K, Hamberg M, Alvelius G, et al. Liquid chromatography-mass spectrometry utilizing multi-stage fragmentation for the identification of oxysterols. J Lipid Res 2007; 48: 976–87.

Liere P, Pianos A, Eychenne B, Cambourg A, Liu S, Griffiths W, et al. Novel lipoidal derivatives of pregnenolone and dehydroepiandrosterone and absence of their sulfated counterparts in rodent brain. J Lipid Res 2004; 45: 2287–302.

Liu S, Sjövall J, Griffiths WJ. Neurosteroids in rat brain: extraction, isolation, and analysis by nanoscale liquid chromatography-electrospray mass spectrometry. Anal Chem 2003; 75: 5835–46.

Lund EG, Guileyardo JM, Russell DW. cDNA cloning of cholesterol 24-hydroxylase, a mediator of cholesterol homeostasis in the brain. Proc Natl Acad Sci USA 1999; 96: 7238–43.

Lund EG, Kerr TA, Sakai J, Li W-P, Russell DW. cDNA cloning of mouse and human cholesterol 25-hydroxylases, polytopic membrane proteins that synthesize a potent oxysterol regulator of lipid metabolism. J Biol Chem 1998; 273: 34316–27.

Lund EG, Xie C, Kotti T, Turley SD, Dietschy JM, Russell DW. Knockout of the cholesterol 24-hydroxylase gene in mice reveals a brain-specific mechanism of cholesterol turnover. J Biol Chem 2003; 278: 22980–8.

Lutjohann D, Breuer O, Ahlborg G, Nennesmo I, Siden A, Diczfalusy U, et al. Cholesterol homeostasis in human brain: evidence for an age-dependent flux of 24S-hydroxycholesterol from the brain into the circulation. Proc Natl Acad Sci USA 1996; 93: 9799–804.

Lütjohann D, Brzezinka A, Barth E, Abramowski D, Staufenbiel M, von Bergmann K, et al. Profile of cholesterol-related sterols in aged amyloid precursor protein transgenic mouse brain. J Lipid Res 2002; 43: 1078–85.

Mast N, Anderson KW, Lin JB, Li Y, Turko IV, Tatsuoka C, et al. Cytochrome P450 27A1 deficiency and regional differences in brain sterol metabolism cause preferential cholestanol accumulation in the cerebellum. J Biol Chem 2017a; 292: 4913–24.

Mast N, Reem R, Bederman I, Huang S, DiPatre PL, Bjorkhem I, et al. Cholestenoic acid is an important elimination product of cholesterol in the retina: comparison of retinal cholesterol metabolism with that in the brain. Invest Ophthalmol Vis Sci 2011; 52: 594–603.

Mast N, Saadane A, Valencia-Olvera A, Constans J, Maxfield E, Arakawa H, et al. Cholesterol-metabolizing enzyme cytochrome P450 46A1 as a pharmacologic target for Alzheimer's disease. Neuropharmacology 2017b; 123: 465–76.

Meaney S, Bodin K, Diczfalusy U, Björkhem I. On the rate of translocation in vitro and kinetics in vivo of the major oxysterols in human circulation: critical importance of the position of the oxygen function. J Lipid Res 2002; 43: 2130–5.

Meaney S, Heverin M, Panzenboeck U, Ekström L, Axelsson M, Andersson U, et al. Novel route for elimination of brain oxysterols across the blood-brain barrier: conversion into 7alpha-hydroxy-3-oxo-4-cholestenoic acid. J Lipid Res 2007; 48: 944–51.

Mellon SH, Griffin LD. Neurosteroids: biochemistry and clinical significance. Trends Endocrinol Metab 2002; 13: 35–43.

Migaud M, Charlesworth P, Dempster M, Webster LC, Watabe AM, Makhinson M, et al. Enhanced long-term potentiation and impaired learning in mice with mutant postsynaptic density-95 protein. Nature 1998; 396: 433–9.

Miller WL, Bose HS. Early steps in steroidogenesis: intracellular cholesterol trafficking. J Lipid Res 2011; 52: 2111–35.

Mitchell JR, Wood E, Collins K. A telomerase component is defective in the human disease dyskeratosis congenita. Nature 1999; 402: 551–5.

Mitroi DN, Pereyra-Gómez G, Soto-Huelin B, Senovilla F, Kobayashi T, Esteban JA, et al. NPC1 enables cholesterol mobilization during long-term potentiation that can be restored in Niemann-Pick disease type C by CYP46A1 activation. EMBO Rep 2019; 20: e48143.

Mueller JW, Gilligan LC, Idkowiak J, Arlt W, Foster PA. The regulation of steroid action by sulfation and desulfation. Endocr Rev 2015; 36: 526–63.

Murai KK, Nguyen LN, Irie F, Yamaguchi Y, Pasquale EB. Control of hippocampal dendritic spine morphology through ephrin-A3/EphA4 signaling. Nat Neurosci 2003; 6: 153–60.

Murakami G, Hojo Y, Kato A, Komatsuzaki Y, Horie S, Soma M, et al. Rapid nongenomic modulation by neurosteroids of dendritic spines in the hippocampus: androgen, oestrogen and corticosteroid. J Neuroendocrinol 2018; 30: e12561.

Narayanan B, Lade JM, Heck CJS, Dietz KD, Wade H, Bumpus NN. Probing ligand structure-activity relationships in pregnane X receptor (PXR): efavirenz and 8-hydroxyefavirenz exhibit divergence in activation. ChemMedChem 2018; 13: 736–47.

Nelson CD, Kim MJ, Hsin H, Chen Y, Sheng M. Phosphorylation of threonine-19 of PSD-95 by GSK-3beta is required for PSD-95 mobilization and long-term depression. J Neurosci 2013; 33: 12122–35.

Nieweg K, Schaller H, Pfrieger FW. Marked differences in cholesterol synthesis between neurons and glial cells from postnatal rats. J Neurochem 2009; 109: 125–34.

Nóbrega C, Mendonça L, Marcelo A, Lamazière A, Tomé S, Despres G, et al. Restoring brain cholesterol turnover improves autophagy and has therapeutic potential in mouse models of spinocerebellar ataxia. Acta Neuropathol 2019; 138: 837–58.

Oakley H, Cole SL, Logan S, Maus E, Shao P, Craft J, et al. Intraneuronal beta-amyloid aggregates, neurodegeneration, and neuron loss in transgenic mice with five familial Alzheimer's disease mutations: potential factors in amyloid plaque formation. J Neurosci 2006; 26: 10129–40.

Ohno M, Chang L, Tseng W, Oakley H, Citron M, Klein WL, et al. Temporal memory deficits in Alzheimer's mouse models: rescue by genetic deletion of BACE1. Neuropsychopharm 2006; 23: 251–60.

Okuda K, Masumoto O, Ohyama Y. Purification and characterization of 5 beta-cholestane-3 alpha, 7 alpha, 12 alpha-triol 27-hydroxylase from female rat liver mitochondria. J Biol Chem 1988; 263: 18138–42.

Patel TK, Patel VB, Rana DG. Possible anti-depressant effect of efavirenz and pro-depressive-like effect of voriconazole in specified doses in various experimental models of depression in mice. Pharmacol Rep 2017; 69: 1082–7.

Patriarchi T, Buonarati OR, Hell JW. Postsynaptic localization and regulation of AMPA receptors and Cav1.2 by β2 adrenergic receptor/PKA and Ca(2+)/CaMKII signaling. EMBO J 2018; 37:

Paul SM, Doherty JJ, Robichaud AJ, Belfort GM, Chow BY, Hammond RS, et al. The major brain cholesterol metabolite 24(S)-hydroxycholesterol is a potent allosteric modulator of N-methyl-D-aspartate receptors. J Neurosci 2013; 33: 17290–300.

Petrov AM, Lam M, Mast N, Moon J, Li Y, Maxfield E, et al. CYP46A1 activation by efavirenz leads to behavioral improvement without significant changes in amyloid plaque load in the brain of 5XFAD mice. Neurotherapeutics 2019a; 16: 710–24.

Petrov AM, Mast N, Li Y, Denker J, Pikuleva IA. Brain sterol flux mediated by cytochrome P450 46A1 affects membrane properties and membrane-dependent processes. Brain Commun 2020; 2: fcaa043.

Petrov AM, Mast N, Li Y, Pikuleva IA. The key genes, phosphoproteins, processes, and pathways affected by efavirenz-activated CYP46A1 in the amyloid-decreasing paradigm of efavirenz treatment. FASEB J 2019b; 33: 8782–98.

Porcu P, Barron AM, Frye CA, Walf AA, Yang S-Y, He X-Y, et al. Neurosteroidogenesis today: novel targets for neuroactive steroid synthesis and action and their relevance for translational research. J Neuroendocrinol 2016; 28.

Ramirez DMO, Andersson S, Russell DW. Neuronal expression and subcellular localization of cholesterol 24-hydroxylase in the mouse brain. J Comp Neurol 2008; 507: 1676–93.

Rosenberger A, Rozemuller A, van der Flier WM, Scheltens P, van der Vies SM, Hoozemans J. Altered distribution of the EphA4 kinase in hippocampal brain tissue of patients with Alzheimer's disease correlates with pathology. Acta Neuropathol Commun 2014; 2: 79.

Sension M, Deckx H. Lipid metabolism and lipodystrophy in HIV-1-infected patients: the role played by nonnucleoside reverse transcriptase inhibitors. AIDS Rev 2015; 17: 21–36.

Sewer MB, Waterman MR. ACTH modulation of transcription factors responsible for steroid hydroxylase gene expression in the adrenal cortex. Microsc Res Tech 2003; 61: 300–7.

Sharma D, Lau AJ, Sherman MA, Chang TKH. Agonism of human pregnane X receptor by rilpivirine and etravirine: comparison with first generation non-nucleoside reverse transcriptase inhibitors. Biochem Pharmacol 2013; 85: 1700–11.

Steiner P, Higley MJ, Xu W, Czervionke BL, Malenka RC, Sabatini BL. Destabilization of the postsynaptic density by PSD-95 serine 73 phosphorylation inhibits spine growth and synaptic plasticity. Neuron 2008; 60: 788–802.

Stone D, Hechter O. Studies on ACTH action in perfused bovine adrenals: site of action of ACTH in corticosteroids. Arch Biochem Biophys 1954; 51: 457–69.

Tang H, Hua F, Wang J, Yousuf S, Atif F, Sayeed I, et al. Progesterone and vitamin D combination therapy modulates inflammatory response after traumatic brain injury. Brain Inj 2015; 29: 1165–74.

Tohyama J, Billheimer JT, Fuki IV, Rothblat GH, Rader DJ, Millar JS. Effects of nevirapine and efavirenz on HDL cholesterol levels and reverse cholesterol transport in mice. Atherosclerosis 2009; 204: 418–23.

Tuckey RC. Progesterone synthesis by the human placenta. Placenta 2005; 26: 273–81.

Vanmierlo T, Weingärtner O, van der Pol S, Husche C, Kerksiek A, Friedrichs S, et al. Dietary intake of plant sterols stably increases plant sterol levels in the murine brain. J Lipid Res 2012; 53: 726–35.

Vigil FA, Mizuno K, Lucchesi W, Valls-Comamala V, Giese KP. Prevention of long-term memory loss after retrieval by an endogenous CaMKII inhibitor. Sci Rep 2017; 7: 4040.

Wikvall K. Hydroxylations in biosynthesis of bile acids. Isolation of a cytochrome P-450 from rabbit liver mitochondria catalyzing 26-hydroxylation of C27-steroids. J Biol Chem 1984; 259: 3800–4.

Zhou Y-Q, Shi Y, Yang L, Sun Y-F, Han Y-F, Zhao Z-X, et al. Genetically engineered distal airway stem cell transplantation protects mice from pulmonary infection. EMBO Mol Med 2020; 12: e10233.